

Central European Journal of Chemistry

Systematic investigation and in vitro biocompatibility studies on mesoporous europium doped hydroxyapatite

Research Article

Cristina L. Popa¹, Carmen S. Ciobanu¹, Simona L. Iconaru^{1,2}, Miruna Stan³, Anca Dinischiotu³, Constantin C. Negrila¹, Mikael Motelica-Heino², Regis Guegan², Daniela Predoi^{1*}

¹National Institute of Materials Physics, 077125 Magurele, Romania

²Institute for Earth Sciences, UMR 7327, CNRS-University of Orléans, 45071 Orléans cedex 02, France

³Department of Biochemistry and Molecular Biology, University of Bucharest, 91-95 Spl. Independentei, 050095, Bucharest, Sector 5, Romania

Received 1 November 2013; Accepted 22 January 2014

Abstract: This paper reports the systematic investigation of europium doped hydroxyapatite (Eu:HAp). A set of complementary techniques, namely Fourier Transform Infrared spectroscopy (FTIR), X-ray photoelectron spectroscopy (XPS), transmission electron microscopy (TEM) and the Brunauer–Emmett–Teller (BET) technique were used towards attaining a detailed understanding of Eu:HAp. The XPS analysis confirmed the substitution of Ca ions by Eu ions in the Eu:HAp samples. Secondly, Eu:HAp and pure HAp present type IV isotherms with a hysteresis loop at a relative pressure (P/P₀) between 0.4 and 1.0, indicating the presence of mesopores. Finally, the *in vitro* biological effects of Eu:HAp nanoparticles were evaluated by focusing on the F-actin filament pattern and heat shock proteins (Hsp) expression in HEK293 human kidney cell line. Fluorescence microscopy studies of the actin protein revealed no changes of the immunolabelling profile in the renal cells cultured in the presence of Eu:HAp nanoparticles. Hsp60, Hsp70 and Hsp90 expressions measured by Western blot analysis were not affected after 24 and 48 hours exposure. Taken together, these results confirmed the lack of toxicity and the biocompatibility of the Eu:HAp nanoparticles. Consequently, the possibility of using these nanoparticles for medical purposes without affecting the renal function can be envisaged.

Keywords: Nanoparticles • Hydroxyapatite • Europium • In vitro studies © Versita Sp. z o.o.

1. Introduction

Hydroxyapatite (HAp), a member of the apatite family, has been the focus of many studies due to its remarkable biocompatibility, bioactivity and osteoconductivity. Being the most important inorganic component of bones and teeth, HAp has the general formula, $Ca_{10}(PO_4)_6(OH)_2$ and constitutes 65% of the total mineral content of the human [1-5]. So far, synthetic HAp has been used for damaged bone reconstruction with promising results. Furthermore, given their non-toxic and non-inflammatory properties, HAp nanostructures are suitable for both bio-imaging and drug delivery. Although several routes can be pursued for the synthesis of HAp, the co-precipitation method has

attracted great attention due to its ability to generate nanoscale particles and nanocrystalline powders at a low processing temperature. This method allows for both size and morphology of the synthesized nanoparticles to be controlled, something of fundamental importance as the process of calcium phosphate deposition can result in the formation of renal stones [6].

One of the most important properties of hydroxyapatite is the ability to incorporate a wide variety of substitutions for Ca²⁺, PO₄³⁻ and/or OH⁻ ions due to the flexibility of the apatite structure. Trivalent europium (Eu) ions have been used as luminescent probes in the investigation of the crystallographic structure of activator centres, as well as a tool to probe the local symmetry and occupancy of the

cationic sites in the apatite structures. Doat et al. showed that Eu3+ ion luminescence can be obtained under visible irradiation [7], and is suitable for prolonged examination of living cells. Previous reports have detailed several synthesis techniques for the study of the substitution of Ca2+ by Eu3+ ions. For example, André et al. [8] obtained Eu-doped hydroxyapatite (Eu:HAp) nanorods with diameters from 9 to 26 nm by using a microwave hydrothermal method, while. Barta et al. reported that Eu³⁺ ions have the potential for the treatment of bone density disorders such as osteoporosis [9]. Furthermore, Chen et al. [10] investigated the toxicity, drug adsorption capacity and sustained diffusion-driven ibuprofen release associated with Eu^{3+/}Gd³⁻ doped HAp nanorods. To this end, the cytotoxicity, drug adsorption and release, as well as in vitro/in vivo MR/luminescence/computed tomography (CT) imaging of Eu³⁺ and Gd dual doped HAp nanorods were investigated, revealing negligable in vitro cell toxicity and high absorbtion capacity. Recently, Boanini et al. [11] provided an overview of the recent results achieved on ion-substituted calcium phosphates prepared at low temperature by direct synthesis in aqueous medium or by hydrolysis of more soluble calcium phosphates. In addition, Ciobanu et al. [12] reported a novel co-precipitation adapted synthesis for europium doped hydroxyapatite (Eu:HAp). This group synthesized europium-doped hydroxyapatite nanoparticles by the co-precipitation method at a low temperature and showed by XRD studies that Eu³⁺ ions have been successfully inserted into HAp. Moreover, their results revealed that the obtained Eu:HAp (x_{E,1}≥0) particles are well assigned to the hexagonal lattice structure of the hydroxyapatite phase and the prepared Eu:HAp samples conserved regular ellipsoidal morphology, thus confirming that doping with Eu3+ has morphology reduced impact.

The aims of this work were to study the effects of Eu^{3+} doping at a wide range of concentrations on the structural morphology and the specific surface area of the synthesized nanoparticles as determined by transmission electron microscopy (TEM) and by BET, respectively. Moreover, this research also focused on a comprehensive understanding of the Eu:HAp samples prepared with various x_{Eu} concentration by employing the X-ray photoelectron spectroscopy (XPS) technique, which was expected to give new insights regarding the insertion of europium cations in the structure of HAp; this is the first time that the latter study has been performed.

Finally, this study is the first to report the effects of europium-doped hydroxyapatite nanoparticles on the morphology and size of human kidney cells (HEK293), as well as characterize the disposition of the actin cytoskeletal filaments and the expression heat shock proteins following exposure. Although it is well known that hydroxyapatite represents a mineral involved in osteogenesis, it is also responsible for nephrolithiasis [13] because an important percent of renal stones contain calcium phosphate in the form of hydroxyapatite [14]. Taking into account that the shape and dimension of hydroxyapatite nanoparticles are important parameters in the process of phosphate renal stones formation [15], this study aims to evaluate the response of renal cells following the exposure to the nanoscale particles obtained by the co-precipitation method.

2. Experimental procedure

2.1. Synthesis of the samples

Europium doped hydroxyapatite, $Ca_{10-x}Eu_x(PO_4)_6(OH)_2$ with x_{Eu} =0 (pure HAp), x_{Eu} =0.01, x_{Eu} =0.02, x_{Eu} =0.2 was synthesized by a co-precipitation method at 100°C mixing $Eu(NO_3)_3$ •6H₂O, $Ca(NO_3)_2$ •4H₂O and $(NH_4)_2$ HPO₄ in deionized water as previously described [12,16].

2.2. Characterization techniques

Transmission electron microscopy (TEM) analyses were carried out using a JEOL 200 CX microscope. The specimen for TEM imaging was prepared from particle suspensions in deionised water. A drop of well-dispersed supernatant was placed on a carbon – coated 200 mesh copper grid, followed by drying the sample at ambient conditions before attaching it to the sample holder on the microscope.

The functional groups present in the prepared nanoparticles and thin films were identified by FTIR using a Perkin Elmer Spectrum BX spectrometer. In order to obtain the nanoparticles spectra, 1% of the nano-powder was mixed and ground with 99% KBr. Tablets of 10 mm diameter were prepared by pressing the powder mixture with a pressure of not more than 0.69×10^5 Pa. The spectrum was recorded in the range of 400 to 4000 cm⁻¹ with 4 cm⁻¹ resolution. The first FTIR spectra were obtained after 256 scans at room temperature (25 ± 0.5°C). The data interpretation was performed as described [17-19].

X-ray photoelectron spectroscopy (XPS) measurements were carried out on a SPECS Multimethod Surface Analysis System using monocromatic Al K α radiation (1486.6 eV). The vacuum in the analyzer chamber was p $\sim 3\times10^{-9}$ torr. The X-rays are emitted by an anti-cathode of Al, U = 12.5 kV, filament emission current I = 20 mA. For charge compensation a FG40 flood gun was used, providing an electron beam of 2 eV and 0.3 mA. The XPS recorded spectrum involved an energy window w = 20 eV with the resolution R = 20 eV, and

with 400 recording channels. The XPS spectra recorded were processed using Spectral Data Processor v2.3 (SDP) software. N_2 adsorption/desorption analysis was performed at 77 K using a Micrometrics model ASAP 2020 analyser. The specific surface area was determined by the Brunauer–Emmett–Teller (BET) method [20]. The pore parameters (pore volume and pore diameter) were evaluated from the desorption branch of the isotherm based on the Barrett–Joyner–Halenda (BJH) model [21]. The mean pore diameter, Dp, was calculated from Dp = 4VT/S [20], where VT is the total volume of pores, and S is the BET surface area.

2.3. Biological studies 2.3.1. Cell culture

The HEK 293 cell line (ATCC CRL-1573), derived from human embryonic kidney cells, was maintained in DMEM medium containing 10% fetal bovine serum, 100 U mL $^{-1}$ penicillin and 100 µg mL $^{-1}$ streptomycin, in a humidified atmosphere (with 5% CO $_2$) at 37°C. The culture medium was changed every 2 days until cells reached confluence and were trypsinized with 0.25% (w/v) Trypsin - 0.53 mM EDTA (Sigma-Aldrich).

2.3.2. F-actin staining

HEK 293 cells were seeded onto six-well plates $(3\times10^4~\text{cells well}^{-1})$ and exposed to 100 µg mL⁻¹ of 0%, 1%, 2% and 20% Europium doped hydroxyapatite. After 24 and 48 hours of treatment, the medium was removed, and the cells were fixed in 4% paraformaldehyde for 20 minutes at 4°C and permeabilized with 0.5% Triton X-100 for 1 hour. After three washes with PBS, the cells were incubated for 30 minutes in PBS containing 20 µg mL⁻¹ phalloidin – FITC (Sigma-Aldrich). The nuclei were counterstained with 2 µg/mL DAPI (Invitrogen). The cells were observed using an Olympus IX71 fluorescent microscope with the excitation wavelengths set to 495 nm and 358 nm, and the emission wavelengths set to 513 nm and 461 nm for FITC and DAPI signal detection, respectively.

2.3.3. Western Blot analysis

For the determination of chaperones (Hsp60, Hsp70 and Hsp90) expression at protein level, Western blot analysis was performed. The cells were cultured in the presence of appropriate medium and after 24 or 48 hours of treatment (25 or 100 µg mL-¹ of 0%, 1%, 2% and 20% Europium doped hydroxyapatite) were harvested in lysis buffer (150 mM NaCl, 1% Triton X-100, 0.5% sodium deoxycholate, 0.1% SDS, 50 mM Tris-HCl, pH 8.0 and protease inhibitor cocktail) and incubated for 30 min on ice. Cell lysates were clarified by centrifugation at 13,000 g for 20 min and

the supernatants collected were boiled (95°C) for 5 min. Equal amounts of total protein were subjected to SDS-polyacrylamide gel electrophoresis. Proteins were transferred to Hybond-PVDF membranes in Tris-glycine buffer (48 mM Tris-HCl, pH 8.3, 39 mM glycine, 20% methanol) using a wet transfer unit (BIO-RAD, USA), and after that, membranes were blocked overnight at 4°C, and incubated with specific mouse monoclonal IgG anti-HSPs (all from Santa Cruz Biotechnology) and anti-β-actin (from Sigma-Aldrich). The Western Blot Chromogenic Immunodetection Kit (INVITROGEN) which contains secondary antibody anti-mouse IgG conjugated with alkaline phosphatase and BCIP/ NBT substrate for alkaline phosphatase were used according to manufacturer's instructions. Densitometry data were analyzed by GelQuantNET software for semi-quantification of HSPs and beta-actin.

Statistical analysis. All experiments were done in triplicate and measurements repeated at least three times. The results were expressed as percent of the control values. Data are represented as mean \pm standard deviation.

3. Results

3.1. Structure, formation and morphology of pure HAp and Eu:HAp

The crystal structure of the prepared samples was verified by X-ray diffraction (XRD) [12]. The XRD patterns of the Eu:HAp, $\mathrm{Ca_{10.x}Eu_x(PO_4)_6(OH)_2}$, with different $\mathrm{x_{Eu}}$ values ($\mathrm{x_{Eu}}$ =0.01, 0.02 and 0.2) and HAp ($\mathrm{x_{Eu}}$ =0) confirmed the hexagonal lattice symmetry (space group P63/m) for all samples. Previous studies [12-22] have shown that all the XRD patterns of Eu:HAp samples and pure HAp can be well indexed as a hexagonal phase agreeing well with the values of the standard ASTM data (JCPDS no. 9-0432) indicating a moncrystalline hydroxyapatite phase.

Fig. 1 displays the HRTEM images, Selected Areas Electron Diffraction (SAED) and size distribution of Eu:HAp nanoparticles with $x_{\rm Eu}$ = 0.02 and confirms that the synthesized samples are well-crystallized even at small values of $x_{\rm Eu}$.

In the HRTEM image (Fig. 1B) the crystalline phase of hydroxyapatite with well-resolved lattice fringes can be observed. The distances (2.81 Å and 1.84 Å) between the adjacent lattice fringes are in accordance with the $\rm d_{211}$ and $\rm d_{213}$ spacing values reported in literature (0.2814 nm and 0.184 nm) (JCPDS no. 09-0432). The HRTEM images of the sample further confirm that the synthesized samples are well crystallized single crystals.

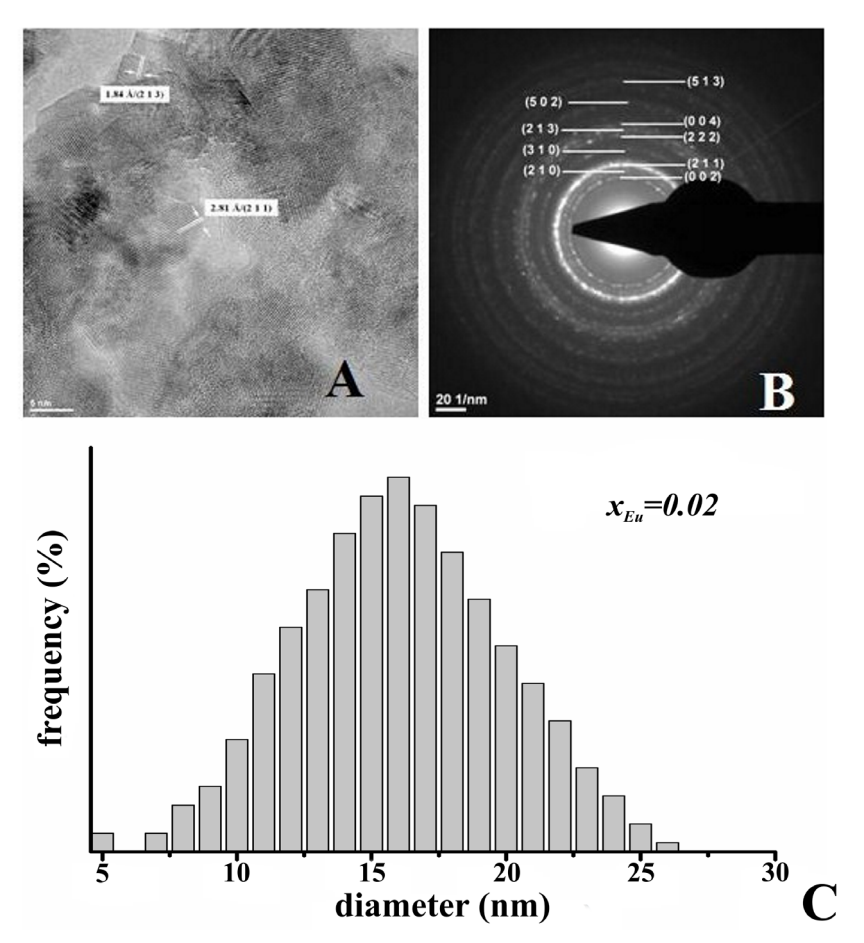


Figure 1. HRTEM image and size distribution of Eu:HAp with $x_{E_0} = 0.02$.

Fig. 2 shows the IR absorbance spectra of Eu:HAp samples with various europium concentrations $(0 \le x_{F_{11}} \le 0.2)$ in the 4000 cm⁻¹ to 400 cm⁻¹ range.

We have previously reported [23] the occurrence of a strong OH⁻ vibration peak (632 cm⁻¹) for all the samples studied. The presence of the broad bands of adsorbed water in the regions 1600–1700 cm⁻¹ and 3200–3600 cm⁻¹ is due to characteristic OH⁻ modes (Fig. 2). Furthermore, recent studies on apatites [24] has described that the band at 3570 cm⁻¹ (stretching) is characterized by the OH⁻ vibrational mode, while the band at 632 cm⁻¹ is a result of an OH⁻ arise from a stretching librational mode.

In agreement with Slosarczyk *et al.* [25], the most noticeable feature of these spectra is the presence of the typical v_4 PO $_4^{3-}$ and v_3 PO $_4^{3-}$ IR vibrations of the phosphate group belonging to apatite in the range from 530–650 cm⁻¹ and 900–1200 cm⁻¹, respectively [26]. The bands around 1090 cm⁻¹ and 1040 cm⁻¹ can be attributed to the v_3 PO $_4$ while the band at 962 arises from v_4 PO $_4$, the 602 cm⁻¹ and 564 cm⁻¹ bands appear from v_4

 PO_4 . Markovik *et al.* [27], suggested that the sharpness of bands, especially that of the 632 cm⁻¹, 602 cm⁻¹ and 564 cm⁻¹ bands, indicates a well-crystallized HAp. The band at 475 cm⁻¹ can be attributed to the $v_2 PO_4$.

Furthermore, in the second derivative spectra the band at 475 cm⁻¹ was identified a $v_2(PO_4^{\ 3-})$. In accordance with previous studies [23,28], the bands assigned in the second derivative spectra of Eu:HAp $(0 \le x_{Eu} \le 0.2)$ can be attributed to molecular vibrations of the phosphate $(PO_4^{\ 3-})$ in an apatitic stoichiometric environment of hydroxyapatite [28].

In the FT-IR spectrum of Eu:HAp with $x_{Eu} \ge 0.1$ (Fig. 2) the bands corresponding to the v_3 vibration of C–O were observed at 1410 cm⁻¹, as characteristic of the carbonate group [29,30].

The intensity of the band located at 1410 cm⁻¹ in the spectrum of Eu:HAp samples with $x_{Eu} \ge 0.1$ is attributed to components of the v_3 mode of a trace amount of CO_3^{2-} . The v_2 vibrations between 850 and 890 cm⁻¹, characteristic of the carbonate group, were not detected because the v_2 CO_3 band at 872 cm⁻¹ is hidden by the

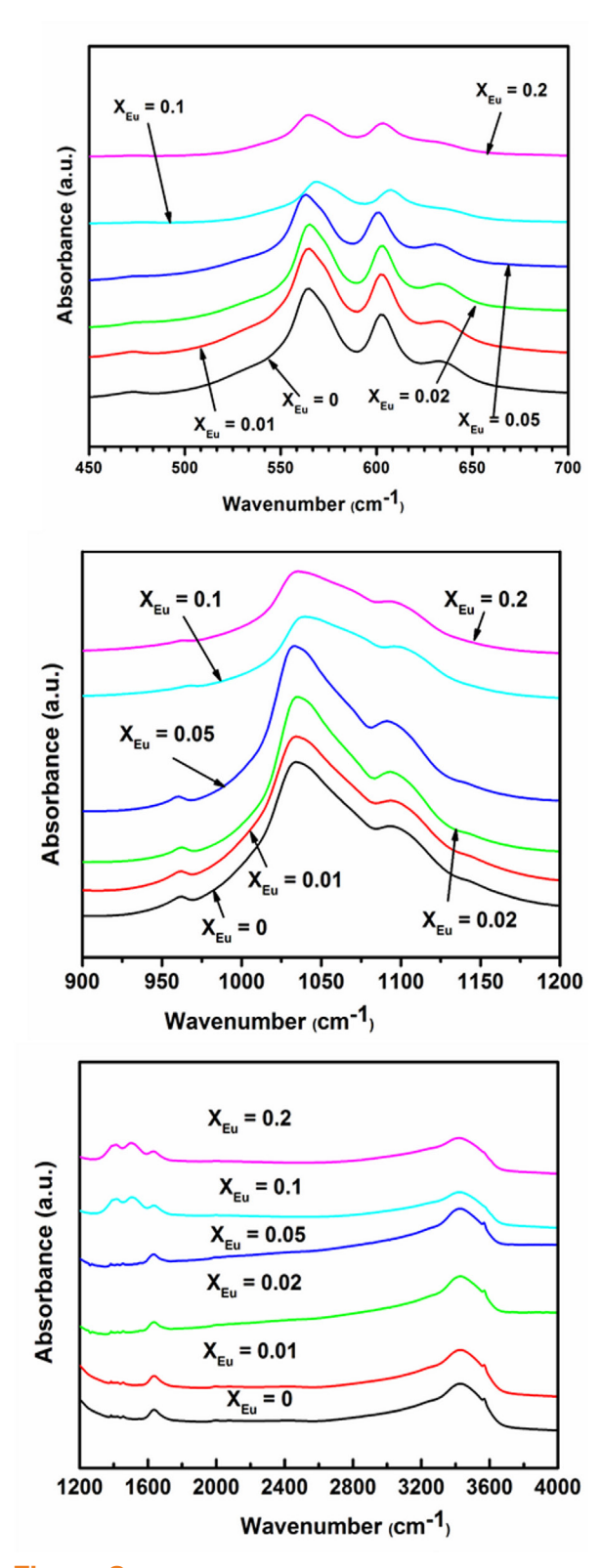


Figure 2. FTIR spectra of europium doped hydroxyapatite (Eu:HAp) with $x_{\rm Eu}$ =0 (black), $x_{\rm Eu}$ =0.01 (red), $x_{\rm Eu}$ =0.02 (green), $x_{\rm Eu}$ =0.05 (dark blue), $x_{\rm Eu}$ =0.1 (light blue) and $x_{\rm Eu}$ =0.2 (purple).

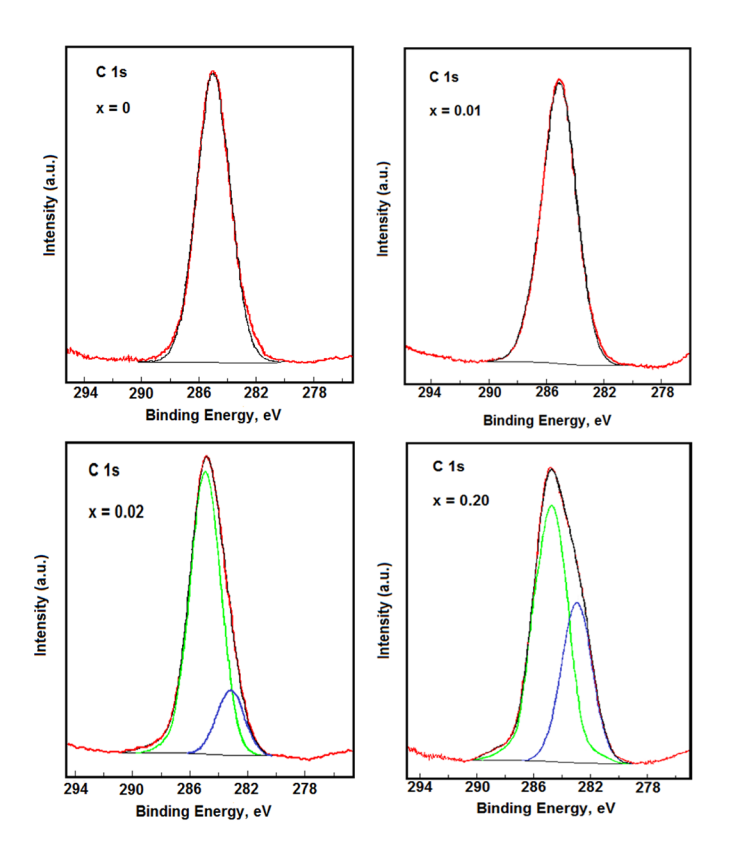
HPO $_4$ band at 875 cm $^{-1}$. A similar situation was described by Markovik *et al.* [27] in their studies on the preparation and comprehensive characterization of calcium hydroxyapatite. Markovik *et al.* and Holcomb *et al.* [31] showed that the CO $_3$ band at 1410 cm $^{-1}$ derives from CO $_3$ ²⁻ (designated as "B-type" carbonate that replaces PO $_4$ ³⁻ ions in the hydroxyapatite lattice). The band at 1510 cm $^{-1}$ was also detected in the FT-IR spectrum of Eu:HAp with $x_{Eu} \ge 0.1$. The band at 1510 cm $^{-1}$ derives from CO $_3$ ²⁻ (designated as "A-type" carbonate that replaces OH $_1$ ions in the hydroxyapatite lattice) [27,32]. In all the spectra pertaining to the Eu:HAp samples, a band at 875 cm $_1$ was detected which is supposed to arise due to HPO $_4$ ²⁻ ions for several reasons [27].

In order to investigate the successful doping of Eu in Eu:HAp, X-ray photoelectron spectroscopy (XPS) measurements were performed. High resolution spectra of the C 1s, Ca 2p, P 2p, O 1s and Eu 3d regions were obtained.

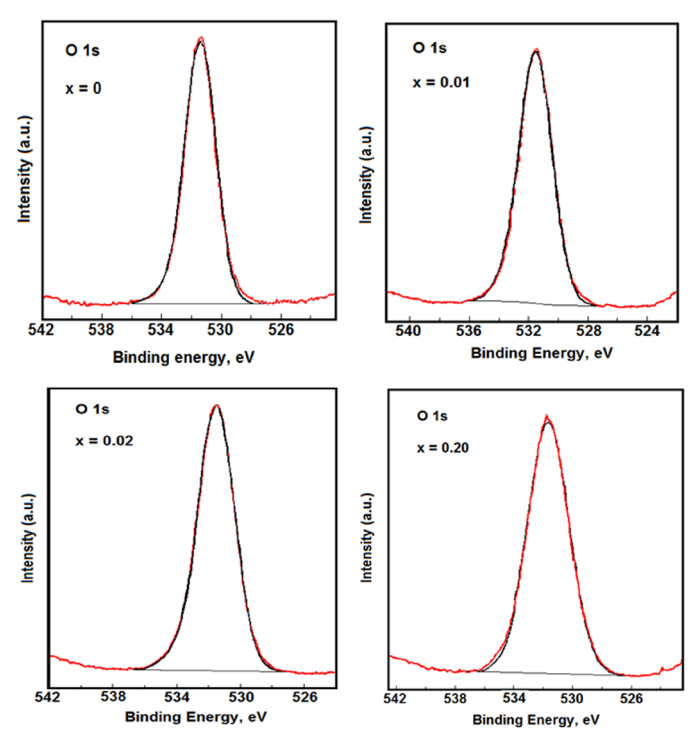
The measured binding energy ($E_{\rm B}$) scale was referenced to a C 1s at the $E_{\rm B}$ value of 284.8 eV [33]. Fig. 3 shows the high–resolution C 1s spectra for the Eu:HAp ($x_{\rm Eu}$ =0.01, $x_{\rm Eu}$ =0.02, $x_{\rm Eu}$ =0.2) and pure HAp ($x_{\rm Eu}$ =0) samples. The decomposition of multiple peaks in the C 1s region was performed and each spectrum had a shoulder on the higher-binding-energy side in addition to the main peak around 284.8 eV. For the samples with $x_{\rm Eu}$ =0.02 and $x_{\rm Eu}$ =0.2 a new peak was observed at around 283.4 eV. The peaks at 284.8 eV and 283.4 eV correspond to residual or adventitious carbon. According to Serra *et al.* [34] the peak positioned at 284.8 eV, corresponds to C–C and C–H bonds.

The peak positioned at 283.4 eV could correspond to C-metal bonds, showing a chemical interaction between Eu and contaminants from the surface layer. The O 1s, Ca 2p, P 2p photoelectron peaks were decomposed according to the binding energies of the carbon bonds in hydroxyapatite [35-36].

Fig. 4 shows the high resolution XPS spectra of oxygen O 1s for Eu:HAp, $Ca_{10-x}Eu_x(PO_4)_6(OH)_2$, with different x_{Eu} values and pure HAp. The peak from 531.4 eV corresponds to hydroxyl groupings resulting from the chemisorption of water or oxygen. These results are in accordance with the previous studies of Moulder *et al.* [37]. The peak position of the hydroxyl ion (OH) was reported as E_B =531.8 eV on a SnO_x surface [38]. In addition, Kawabe *et al.* [39] consider that two oxygen species, *i.e.*, O- and OH-, may be included in the resolved peak at 531.2 eV. Furthermore, the peak position of chemisorbed oxygen species O- on nickel was reported as the binding energy, E_B =531.0-531.5 eV [40-42]. Fig. 5 presents the high-resolution Ca 2p spectra for Eu:HAp (x_{Eu} =0.01, x_{Eu} =0.02, x_{Eu} =0.2) and



 $\textbf{Figure 3.} \ \, \text{High-resolution XPS spectra and curve-fitting results of carbon C 1s for Eu:HAp } (\textbf{x}_{Eu} = 0.01, \textbf{x}_{Eu} = 0.02, \textbf{x}_{Eu} = 0.2) \text{ and pure HAp } (\textbf{x}_{Eu} = 0) \text{ samples.}$



 $\textbf{Figure 4.} \ \ \text{High-resolution XPS spectra and curve-fitting results of oxygen O 1s for Eu: HAp } \\ (x_{Eu} = 0.01, x_{Eu} = 0.02, x_{Eu} = 0.2) \ \ \text{and pure HAp } \\ (x_{Eu} = 0.01, x_{Eu} = 0.02, x_{Eu} = 0.02, x_{Eu} = 0.02) \\ (x_{Eu} = 0.01, x_{Eu} = 0.02, x_{Eu} = 0.02, x_{Eu} = 0.02, x_{Eu} = 0.02) \\ (x_{Eu} = 0.01, x_{Eu} = 0.02, x_{Eu} = 0.02, x_{Eu} = 0.02, x_{Eu} = 0.02, x_{Eu} = 0.02) \\ (x_{Eu} = 0.01, x_{Eu} = 0.02, x_{Eu} = 0.02, x_{Eu} = 0.02, x_{Eu} = 0.02) \\ (x_{Eu} = 0.01, x_{Eu} = 0.02, x_{Eu} = 0.02, x_{Eu} = 0.02, x_{Eu} = 0.02) \\ (x_{Eu} = 0.01, x_{Eu} = 0.02, x_{Eu} = 0.02, x_{Eu} = 0.02, x_{Eu} = 0.02) \\ (x_{Eu} = 0.01, x_{Eu} = 0.02, x_{Eu} = 0.02, x_{Eu} = 0.02, x_{Eu} = 0.02) \\ (x_{Eu} = 0.01, x_{Eu} = 0.02, x_{Eu} = 0.02, x_{Eu} = 0.02, x_{Eu} = 0.02) \\ (x_{Eu} = 0.01, x_{Eu} = 0.02, x_{Eu} = 0.02, x_{Eu} = 0.02, x_{Eu} = 0.02) \\ (x_{Eu} = 0.01, x_{Eu} = 0.02, x_{Eu} = 0.02$

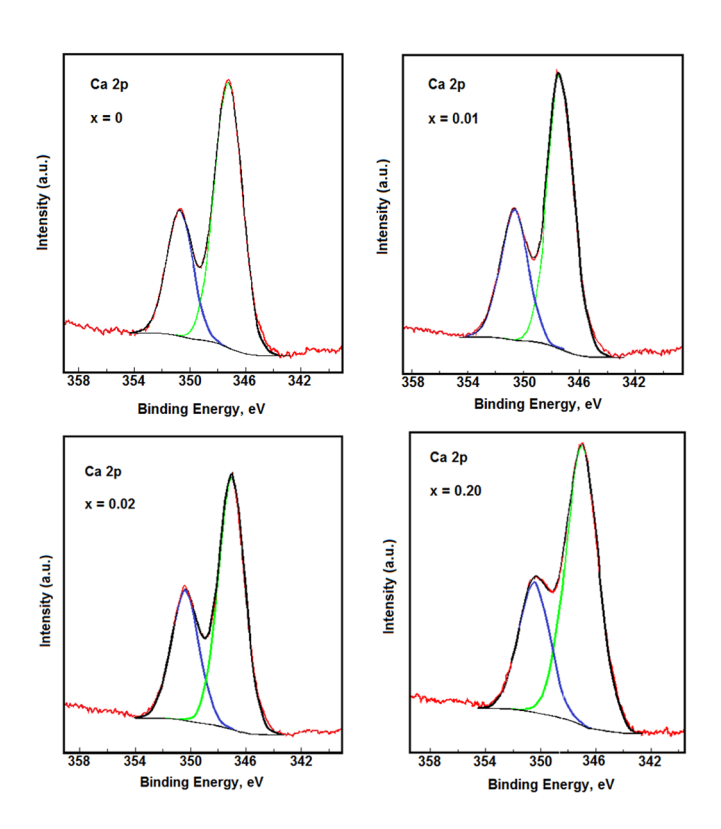


Figure 5. High-resolution XPS spectra and curve-fitting results of calcium Ca 2p for Eu:HAp (x_{Eu}=0.01, x_{Eu}=0.02, x_{Eu}=0.02) and pure HAp (x_{Eu}=0) samples.

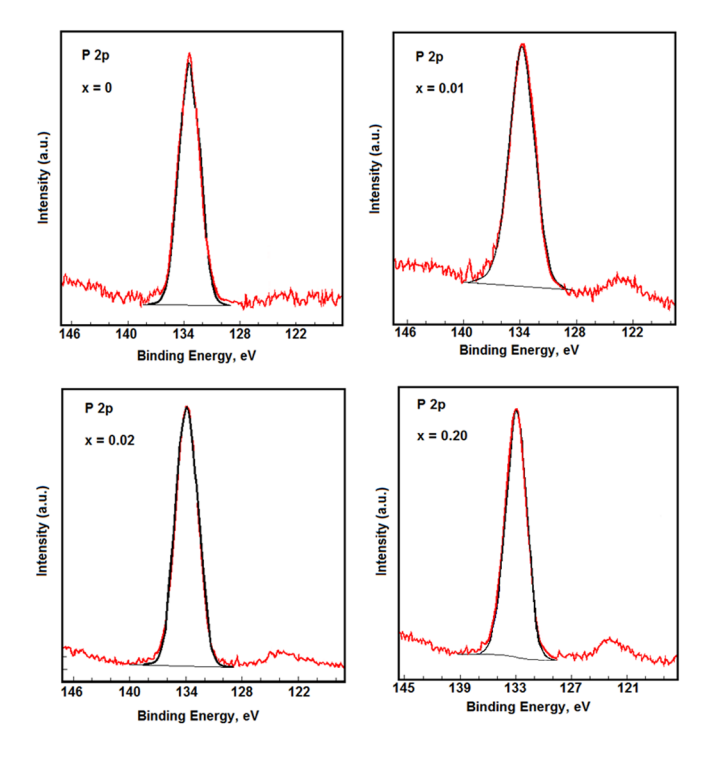


Figure 6. High-resolution XPS spectra and curve-fitting results of phosphorous P 2p for Eu:HAp $(x_{Eu}=0.01, x_{Eu}=0.02, x_{Eu}=0.2)$ and pure HAp $(x_{Eu}=0)$ samples.

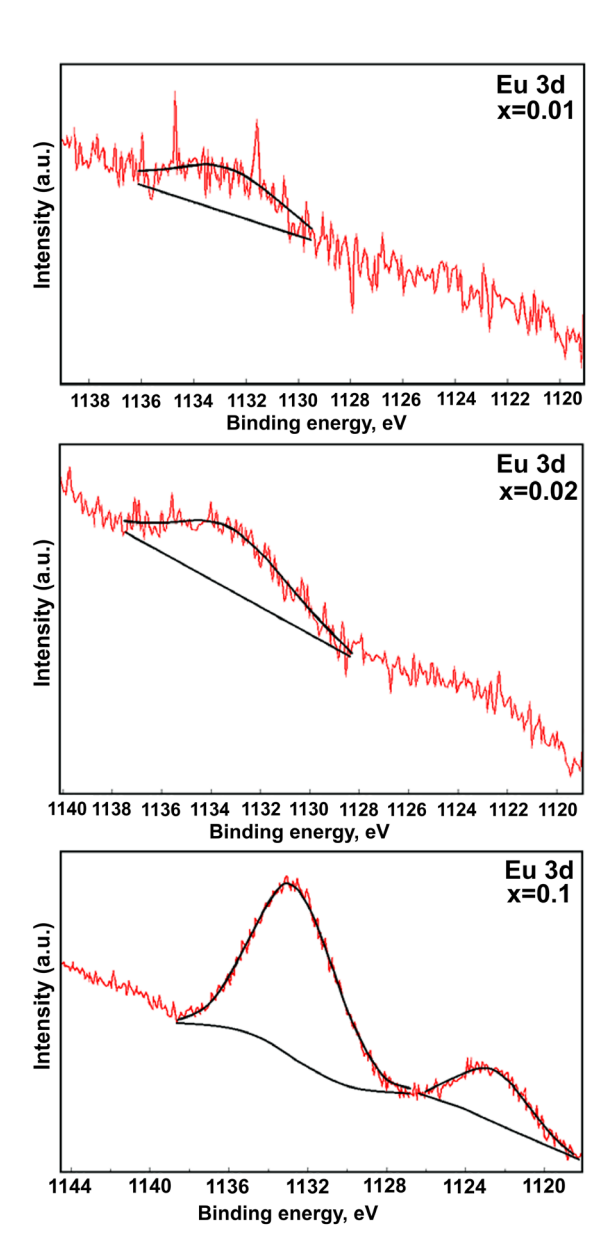


Figure 7. High-resolution XPS spectra and curve-fitting results of phosphorous Eu 3d for Eu:HAp $(x_{Eu}=0.01, x_{Eu}=0.02, x_{Eu}=0.2)$ samples.

pure HAp (x_{Eu} =0) samples. The Ca 2p band of the asprepared samples exhibited a well-resolved doublet with a Ca $2p_{_{3/2}}$ component and a Ca $2p_{_{1/2}}$ component. With increasing europium concentration, the binding energies shift slightly from 347.2 eV for the pure HAp (x_{Eu} =0) to 347.7 eV for the Eu:HAp (x_{Eu} =0.2). The peak located at about 347.2 eV shows that the calcium atoms are bound to a phosphate group (PO $_4$ ³⁻). The shift towards higher binding energy for the Eu:HAp samples indicates that the amount of crystalline HAp has increased.

Following the processing of the deconvolution data, the P 2p photoelectron line consists of one single peak,

at around E_B =133.1eV for pure HAp (x_{Eu} =0) and Eu:HAp (x_{Eu} =0.01, x_{Eu} =0.02 and x_{Eu} =0.2) samples [44]. The high-resolution XPS spectra and curve-fitting results of phosphorous P 2p for Eu:HAp and pure HAp samples are presented in Fig. 6. Stoica *et al.* showed [45] that the P 2p photoelectron line consists of a single peak at the E_B position of 133.4 eV. Moreover, in agreement with previous XPS studies reported [46], the binding energy of the photoelectron peaks for Ca and P are characteristic of their full oxidation states (Ca²+ and P⁵+) for hydroxyapatite.

The high-resolution XPS spectra of the Eu 3d region (Fig. 7) shows the presence of europium in the form of Eu³+ in the Eu:HAp (x_{Eu} =0.01, x_{Eu} =0.02, x_{Eu} =0.2) samples. For Eu 3d $_{3/2}$ the peak appears at a binding energy of 1136.5 eV. These results indicate that europium ions were successfully incorporated into the HAp lattice. The Ca/P ratios were 1.67 for the nanocrystalline pure HAp (x_{Eu} =0) and 1.64 for the europium doped hydroxyapatite (Eu:HAp). In agreement with Nathanael *et al.* [47] the decrease of Ca/P ratio in the Eu:HAp can unequivocally be linked to the substitution of Ca ions by Eu ions.

The porosity of the Eu:HAp and pure HAp samples was measured using the nitrogen physisorption technique. Fig. 8 shows the representative adsorption–desorption isotherms of the Eu:HAp with different x_{Eu} values (x_{Eu} =0.01, 0.02 and 0.2) and HAp (x_{Eu} =0). All the samples show type IV isotherms [48], with a hysteresis loop at a relative pressure (P/P₀) between 0.4 and 1.0, indicating the presence of mesopores. For all the samples the shape of the hysteresis loop is of type H1 which coincides with the properties of typical mesoporous materials [49].

As previously described [50,51], these mesopores are usually formed due to the clustering of primary crystallites. As shown in Fig. 8, the order of BET specific surface areas and Langmuir specific surface areas are as follows: Eu:HAp (x_{Eu} =0.2) > Eu:HAp (x_{Eu} =0.02) > Eu:HAp (x_{Eu} =0.01)>HAp (x_{Eu} =0). The pore size distributions measured using the BJH method is presented in Fig. 9. The maximum BET surface area, Langmuir surface area, and the maximum pore volume obtained were 130.21 m² g¹, 192.091 m² g¹ and 0.49 cm³ g¹, respectively for the samples of Eu:HAp with x_{Eu} =0.2. The average pore diameter value, Dp, increases from 5.61 to 7.83 nm when x_{Eu} increases. The properties of the tested samples are summarized in Table 1.

3.2. Biological studies

Our previous biocompatibility studies of Eu doped crystalline hydroxyapatite bioceramics [22] showed no significant decrease of viability of the HEK293 cells

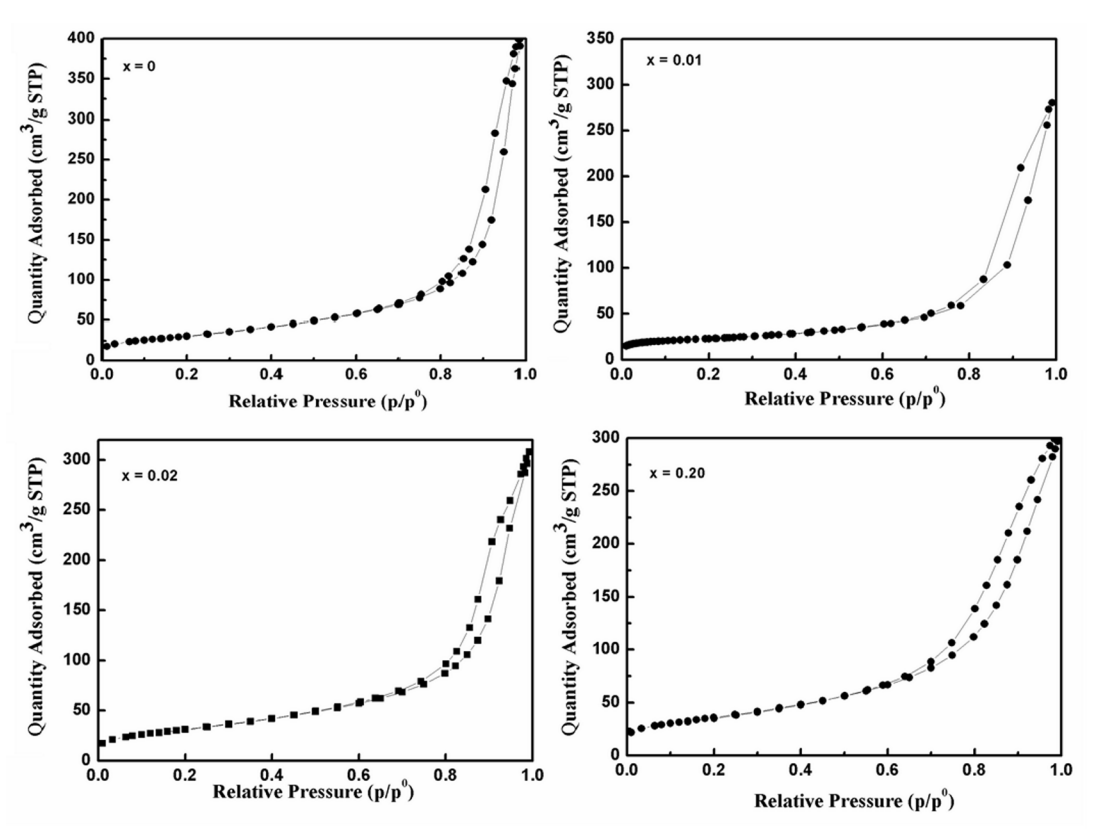


Figure 8. N_2 adsorption–desorption isotherms of Eu:HAp (x_{Eu} =0.01, x_{Eu} =0.02, x_{Eu} =0.2) and pure HAp (x_{Eu} =0) samples.

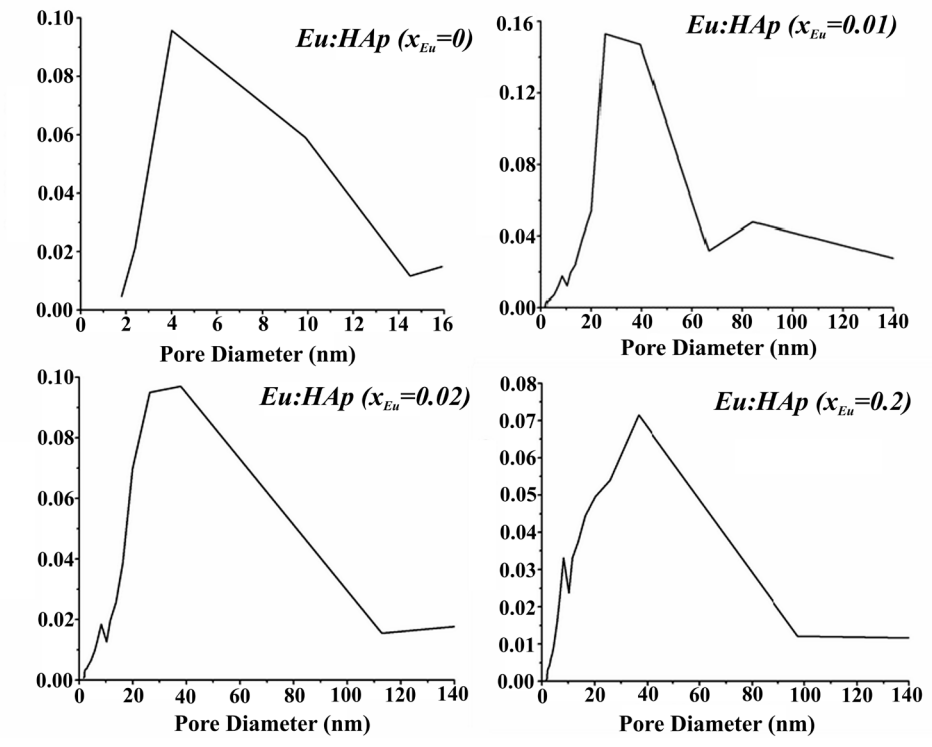


Figure 9. Pore size distribution of Eu:HAp $(x_{Eu}=0.01, x_{Eu}=0.02, x_{Eu}=0.2)$ and pure HAp $(x_{Eu}=0)$ samples.

Table 1. BET surface area, Langmuir surface area, pore size and pore volume of Eu:HAp samples and pure HAp.

Samples	X _{Eu}	BET surface area (m² g ⁻¹)	Langmuir surface area (m² g⁻¹)	Pore size (nm)	Pore volume (cm³ g-¹)	D _թ (nm)
	0.01	112.90	167.72	22.04	0.43	5.07
Eu:HAp	0.02	115.96	171.26	16.56	0.48	5.61
	0.20	130.21	192.091	14	0.49	6.74
HAp	0	71.88	107.27	24.36	0.41	7.83

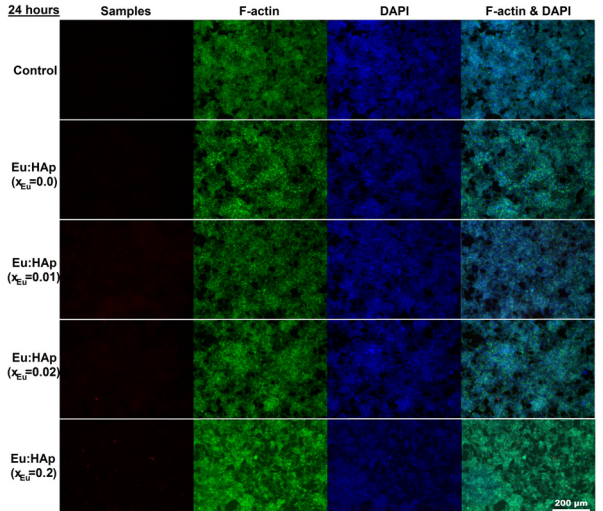


Figure 10. Fluorescence images of HEK293 cells cultured in the presence of 100 μ g mL¹ of Eu:HAp (x_{Eu} =0.01, x_{Eu} =0.02, x_{Eu} =0.2) for 24 hours. Actin cytoskeleton of cells, stained with phalloidin-FiTC (green), shows an appropriate morphology. The nuclei were counterstained with DAPI (blue).

and low levels of intracellular lipid peroxidation in the Eu-doped HAp treated cells. In order to visualize how Eu-doped hydroxyapatite influences the adhesion and proliferation of HEK293 cells, a phalloidin-FITC staining for F-actin was performed. F-actin is a highly conserved and abundant cytoskeletal protein in eukaryotic cells. It is implicated in maintaining the cellular architecture and mediating cell movements [52]. As shown in Figs. 10 and 11, the cell proliferation was not affected after 24 or 48 hours of Eu-doped HAp exposure. The cells adopted a normal morphology, each maintaining contact with the surrounding cells.

It is notable that the cells are not disturbed by the presence of this type of hydroxyapatite, maintaining a healthy morphology and good adhesion.

Moreover, it can also be remarked that the proliferative capacity of these cells was not affected compared to control cells.

Heat shock proteins, Hsp60, Hsp70 and Hsp90 are molecular chaperones, and their expression is up

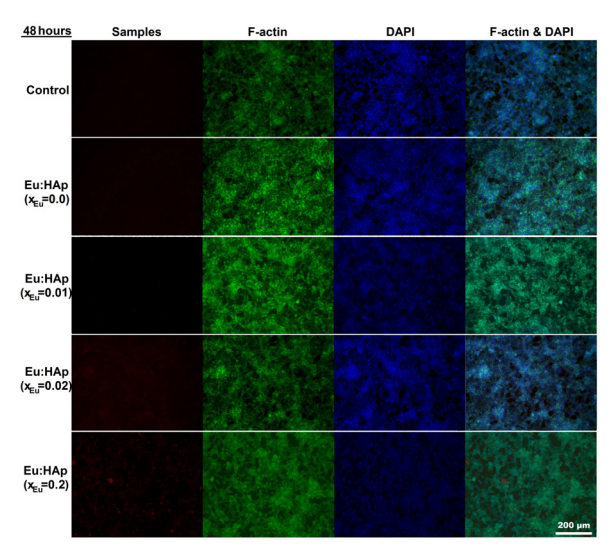


Figure 11. Fluorescence images of HEK293 cells cultured in the presence of 100 μ g mL⁻¹ of Eu:HAp (x_{Eu}=0.01, x_{Eu}=0.02, x_{Eu}=0.2) for 48 hours. Actin cytoskeleton of cells, stained with phalloidin-FITC (green), shows an appropriate morphology. The nuclei were counterstained with DAPI (blue).

regulated under many kinds of stresses, such as heat or chemical toxicity [53].

As shown in Fig. 12, cells exposed to different types and concentration of Eu doped HAp showed no important modifications of Hsp60, Hsp70 and Hsp90 expression compared to control cells.

4. Discussion

In recent years, hydroxyapatite has been of significant interest for the pharmaceutical, biological and medical fields [9, 54] due to its biocompatible and osteoconductive properties [55,56]. Based on the flexibility of the apatitic structure, HAp can incorporate a wide variety of substitutions for Ca²⁺, PO₄³, and/or OH⁻ ions [57-61]. Since Eu³⁺ has a similar ionic radius to Ca²⁺, HAp is a good host for Eu³⁺. The substitution of Ca²⁺ by an Eu³⁺ ion has been achieved by various methods of synthesis such as the solvothermal method [62], a combination of

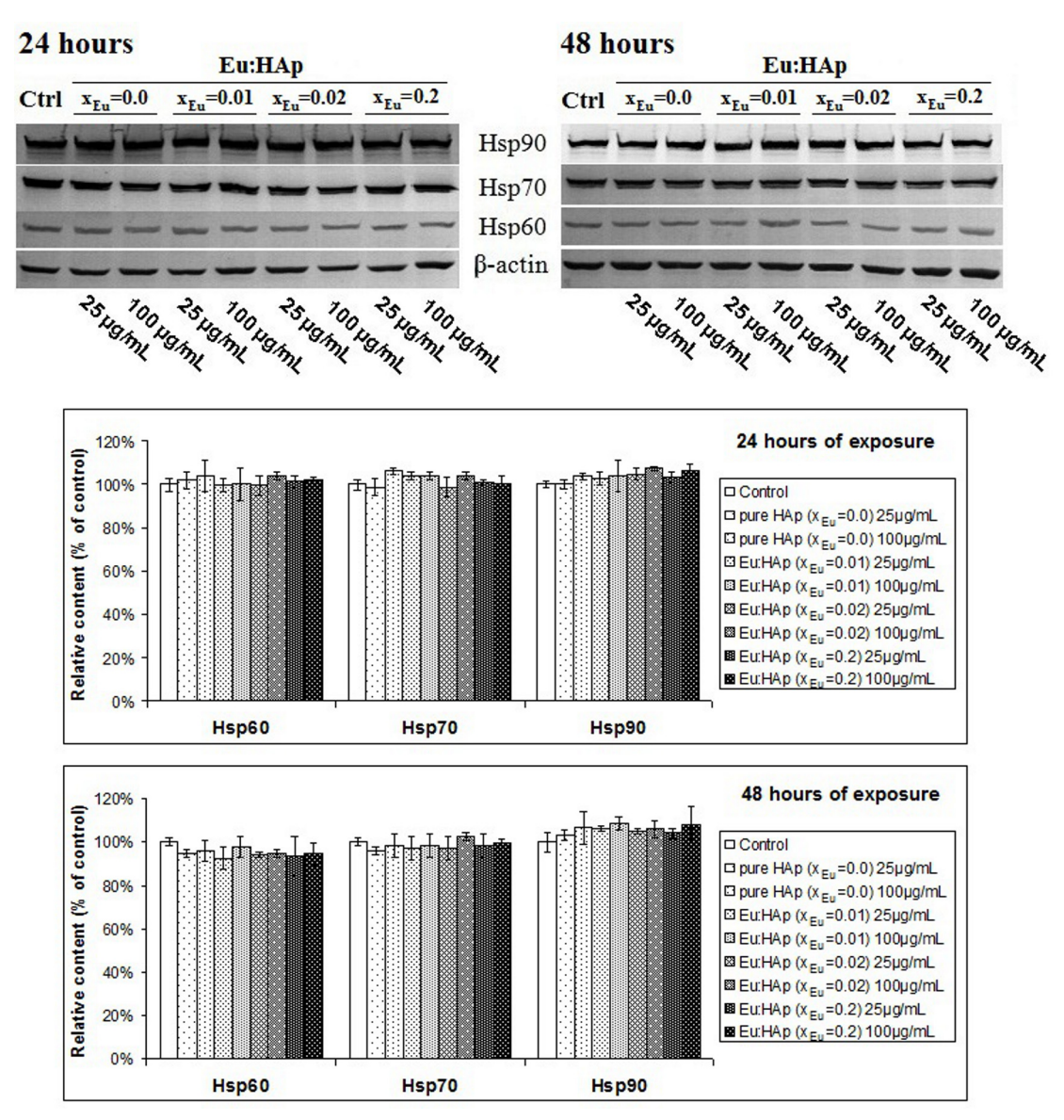


Figure 12. Western blot analysis of Hsp60, Hsp70 and Hsp90.

the sol–gel and electrospinning processes [63]. André et al. [8] obtained Eu-doped hydroxyapatite nanorods by HTMW method at 140°C for 0, 1, 20 or 40 minutes. On the other hand, based on the flexibility of the apatitic structure Gibson et al. [64] succeeded in preparing silicon-substituted hydroxyapatite by the aqueous precipitation method.

For this study, we synthesized the mesoporous and luminescent europium doped hydroxyapatite (Eu:HAp) powders with different concentrations (x_{Eu} =0, x_{Eu} =0.01, x_{Eu} =0.02, x_{Eu} =0.2) by the co-precipitation method at a low temperature. Our previous XRD studies [12,22] have shown that no other secondary phase such as calcium carbonate and/or europium oxide can be detected in

XRD patterns. The results of the XRD studies indicated that pure Eu:HAp nanoparticles were obtained by the simple co-precipitation method. The HRTEM images and Selected Areas Electron Diffraction (SAED) of Eu:HAp nanoparticles confirms that the synthesized samples are well-crystallized single crystals even at small values of \mathbf{x}_{Eu} .

In FTIR analysis, we observed that the contribution of the area that corresponds to the phosphate bands decreases when the Eu concentration in the samples increases. The bands at 475 and 962 cm⁻¹ progressively disappear with the increase of europium concentration. When x_{Eu} =0.2, the bands at 475 and 962 cm⁻¹ are almost absent. We can also observe in the Eu:HAp spectra

a broadening of peak vibration with the decrease of the europium concentration. This behaviour was also observed by Owada *et al.* [65] in sintered Y-doped hydroxyapatite.

The XPS results of the surface composition of the studied samples are in accordance with previous results obtained by Yang et al. [62]. This is the first comprehensive study in which a surface sensitive technique, XPS, has been employed to confirm the substitution of Ca2+ by Eu3+ into HAp. The analysis showed that when europium is present (Eu:HAp) the binding energies of Ca, P and O do not change when compared to the ones of pure HAp $(x_{E_{II}}=0)$. On the other hand, the changes in the atomic percentages of the elements suggest a possible substitution of Ca by Eu. Regarding the Ca2p, P2p and O1s bands, there was no noticeable variation of their position when europium is present. The XPS results show that the P/O ratio remains relatively constant, the Ca/P ratio decreased while the Eu/Ca ratio increased. The (Ca+Eu)/P ratio obtained for the Eu:HAp $(x_{E_{11}}=0.01, x_{E_{11}}=0.02, x_{E_{11}}=0.2)$ sample is practically the same as the Ca/P ratio of pure HAp $(x_{FII}=0)$. The fact that the P/O ratio is relatively constant in all the samples indicates that there was little or no loss of phosphate from the surface.

The results of the nitrogen adsorption/desorption analysis indicates that the doping of Eu³⁺ has not altered the basic pore structure of the mesoporous HAp but improved the specific surface area of about 60% for low concentration to 100% for the highest concentration of Eu

In addition, our study has demonstrated that in the cells treated with different types and concentrations of Eu doped HAp nanoparticles for 24 and 48 hours, the F-actin distribution was normal. To be more specific, F-actin resided around the nuclei and extended until the periphery of HEK293 cells, which is in accordance with previous data [66,67]. Moreover, the F-actin pattern was the same for control and exposed cells, which suggested a very low or a lack of toxicity of these types of nanoparticles.

The induction of stress response proteins is highly conserved and protects different cells against several types of stresses [68]. Among the various stress response pathways, the gene expression and synthesis of different heat shock protein family members, such as Hsp 60, Hsp70 and Hsp 90, are some of the key cellular processes [69]. In non-stressed conditions, these proteins function as molecular chaperones, maintaining and facilitating protein conformation and transport. In response to stress, heat shock proteins expression counteracts protein aggregation, promotes the degradation of highly denatured proteins and refolds

the misfiled proteins or with damaged three dimensional structures [70].

The Hsp70 chaperone systems play an essential role in hostile environments as well as under normal conditions. These are the most highly conserved and first to be induced in the presence of stressors [71]. The increased levels of Hsp70 have been considered to resulting due to the action of xenobiotics and/or their metabolites which have not been scavenged by detoxification processes and have affected the three dimensional structure of native proteins [72]. Several studies revealed that metal based nanoparticles induced toxicity in a cell type dependent manner and the protein expression of Hsp70 was up-regulated [73,74]. Members of Hsp70 are found in the cytosol, nucleus, endoplasmic reticulum and mitochondrion [75]. The members of the Hsp 60 protein family, mainly located in the mitochondria and coded by the nuclear genome, play a significant role in polypeptide folding and in protein translocation [76]. At the same time, Hsp90 is the most abundant cytosolic heat shock protein family in eukaryotic cells and a decrease in its concentration is correlated with mortality in mammalian cells [71]. Recently, an increase of Hsp90 expression was noticed when melanoma targeted magnetite nanoparticles conjugated with a melanogenesis substrate were used [77].

Previous studies reported that in the cells exposed to hydroxiapatite based nanoparticles, a stress was developed [78-79]. This could be counteracted by an up-regulation of Hsps expression [74,77]. Contrary to these observations, our study revealed no significant alteration of Hsp60, Hsp70 and Hsp90 expression.

Based on the direct correlation between the level of stress and the protein expression of Hsps, it seems that the level of toxicity induced in HEK293 cells by the exposure to these nanoparticles was low or absent. These results were valid for all concentrations of Eu doped HAp tested in this study and were not europium level dependent.

5. Conclusion

The results presented in this paper show the influence of the europium doping on hydroxyapatite bioceramics prepared by the co-precipitation method. XPS analysis indicated that Eu was able to quickly substitute Ca into HAp by the co-precipitation method. High-resolution XPS analysis of the key elements of as-prepared samples, Ca, P, O and Eu indicated that distinctive photoelectron peaks could be attributed to the presence of Eu in the as-prepared samples with x_{Eu} =0.01, x_{Eu} =0.02, x_{Eu} =0.2. Europium did not change the chemistry or morphology

of the pure HAp. After the europium doping of the hydroxyapatite, the BET specific surface area of the asprepared samples increased from pure HAp to Eu:HAp with x_{Eu} =0.20. The as-prepared Eu:HAp samples exhibit mesoporous structure, which could prove suitable as a drug delivery system.

The lack of cytotoxic effect on actin organisation and no stress response initiation in cells were highlighted. It seems that the cell compatibility with these Eu:HAp bioceramics correlates very well with its structure and nanodimension.

Taken together, the normal aspect of F-actin filaments organization and heat shock proteins expression that remained almost unchanged support the idea that these

Eu-doped HAp samples were not toxic and provided good conditions for cell proliferation. These sustain the applicability of europium-doped hydroxyapatite for medical purposes.

Acknowledgments

The authors would like to thank Dr. F. Frumosu for XPS measurements and Dr. B.S. Vasile for TEM measurements. The financial and encouragement support provided by the Ministery of Educations of Romania under the project IFA-CEA No. C2-06.

References

- [1] R. Cortesi, C. Nasturzzi, S.S. Davis, Biomaterials 19, 1641 (1998)
- [2] P. Yang , Z. Quan, C. Li, X. Kang, H. Lian, J. Lin, Biomaterials 29, 4341(2008)
- [3] S.L. Iconaru, A.M. Prodan, P. Le Coustumer, D. Predoi, J. Chem., doi:10.1155/2013/412079
- [4] C.S. Ciobanu, S.L. Iconaru, P. Le Coustumer, L.V. Constantin, D. Predoi, Nanoscale Res. Lett. 7, 324 (2012)
- [5] C.S. Ciobanu, S.L. Iconaru, I. Pasuk, B.S. Vasile, A.R. Lupu, A. Hermenean, A. Dinischiotu, D. Predoi, Mater. Sci. Eng. C 33(3), 1395 (2013)
- [6] A.M. Beshensky, J.A. Wesson, E.M. Worcester, J. Am. Soc. Nephrol. 12, 2108 (2001)
- [7] A. Doat, M. Fanjul, F. Pellé, E. Hollande, A. Lebugle, Biomaterials 24, 3365 (2003)
- [8] R.S. André, E.C. Paris, M.F.C Gurgel, I.L.V. Rosa, C.O. Paiva-Santos, M.S. Li, J.A. Varela, E. Longo, J. Alloys Compd. 531, 50 (2012)
- [9] C.A. Barta, K. Sachs-Barrable, J. Jia, K.H. Thompson, K.M. Wasan, C. Orvig, Dalton Trans. 21(43), 5019 (2007)
- [10] F. Chen, P. Huang, Y.J. Zhu, J. Wu, C.L. Zhang, D.X. Cui, Biomaterials 32, 9031 (2011)
- [11] E. Boanini, M. Gazzano, A. Bigi, Acta Biomater. 6, 1882 (2010)
- [12] C.S. Ciobanu, S.L. Iconaru, F. Massuyeau, L.V. Constantin, A. Costescu, D.Predoi, J. Nanomater. doi:10.1155/2012/94280 (2012)
- [13] H.G. Tiselius, I. Hojgaard, A.M. Fornander, M.A. Nilsson, Urolithiasis (Millet the Printer Inc., Dallas, 1996)
- [14] N.S. Mandel, G.S.Mandel, J. Urol. 142, 1516 (1989)
- [15] M. Zelenková, O. Sohnel, F. Grases, Urology 79(4), (2012)

- [16] C.S. Ciobanu, E. Andronescu, B.S. Vasile, C.M. Valsangiacom, R.V. Ghita, D. Predoi, J. Optoelectron Adv. Mat. 4(10), 1515 (2010)
- [17] J. Kolmas, A. Jaklewicz, A. Zima, M. Bućko, Z. Paszkiewicz, J. Lis, A. Ślosarczyk, W. Kolodziejski, J. Mol. Struct. 987, 40 (2011)
- [18] B. Matsuhiro, P. Rivas, J. Appl. Phycol. 5, 45 (1993)
- [19] E. Gómez-Ordóñez, P. Rupérez, Food Hydrocolloids 25, 1514 (2011)
- [20] S. Brunauer, P.H. Emmett, E. Teller, J. Am. Chem. Soc. 60(2), 309 (1938)
- [21] E.P. Barret, P.B. Joyner, P. Halenda, J. Am. Chem. Soc. 73, 373 (1951)
- [22] C.S. Ciobanu, F. Massuyeau, E. Andronescu, M.S. Stan, A. Dinischiotu, D. Predoi, Dig. J. Nanomater. Bios. 6(4), 1639 (2011)
- [23] S.L. Iconaru, M. Motelica-Heino, D. Predoi, J. Spectros. doi:10.1155/2013/284285 (2013)
- [24] B.O. Fowler, Infrared studies of apatites. I. Inorg. Chem. 13, 194 (1974)
- [25] A. Slosarczyk, Z. Paszkiewicz, C. Paluszkiewicz, J. Mol. Struct. 744–747, 657 (2005)
- [26] M. Lebon, I.Reiche, F.Fröhlich, J.-J.Bahain, C.Falguères, Anal. Bioanal. Chem. 392, 1479 (2008)
- [27] M. Markovik, B.O. Fowler, M.S. Tung, J. Res. Natl. Inst. Stan. 109, 553 (2004)
- [28] C. Castro Ribeiro, I. Gibson, M.A. Barbosa, Biomaterials 27, 1749 (2006)
- [29] K. Nakamoto, Infrared and Raman Spectra of Inorganic and Coordination Compounds, 3rd edition (John Wiley and Sons, New York, 1978)
- [30] R.Z. LeGeros, G. Bonel, R. Legros, Calcif. Tissue Res. 26, 111 (1978)

- [31] D.W. Holcomb, R.A. Yung, Calcif. Tissue Int. 31, 189 (1980)
- [32] J.C. Elliott, PhD Thesis (London University, London, 1974)
- [33] D.A. Lopez, S.R. de Sanchez, S.N. Simison, Electrochim. Acta. 48(7), 845 (2003)
- [34] J. Serra, P. Gonzalez, S. Liste, C. Serra, S. Chiussi, B. Leon, M. Perez-Amour, H.O. Ylanen, M. Hupa, J. Non-Cryst. Solids. 332, 20 (2003)
- [35] K. McLeod, S. Kumar, R. St. Claire Smart, N.K. Dutta, N.H. Voelcker, G.I. Anderson, R. Sekel, Appl. Surf. Sci. 253, 2644 (2006)
- [36] M. Yoshinari, Y. Oda, H. Ueki, S. Biomaterials 22(7), 709 (2001).
- [37] J.F. Moulder, W.F. Stickle, P.E. Sobol, K.D. Bomben, Handbook of X-ray Photoelectron Spectroscopy (Physical Electronics Inc., Minnesota, USA, 1995)
- [38] G. Gaggiotti, A. Galdikas, S. Kaciulis, G. Mattongo, A.Setkus, J. Appl. Phys. 76(8), 4467 (1994)
- [39] T. Kawabe, S. Shimomura, T. Karasuda, K. Tabata, E. Suzuki, Y. Yamaguchi, Surf. Sci. 448, 101 (2000)
- [40] M.S. Hegde, M. Ayyoob, Surf. Sci. 173(2-3), L635 (1986)
- [41] C.N.R. Rao, V. Vijayakrishnan, G.U. Kulkarni, M.K. Rajumon, Appl. Surf. Sci. 84, 285 (1995)
- [42] G.U. Kulkarni, C.N.R. Rao, M.W. Roberts, Langmuir 11, 2572 (1995)
- [43] S. Kaciulis, G. Mattogno, L. Pandolfi, M. Cavalli, G. Gnappi, A. Montenero, Appl. Surf. Sci. 151, 1 (1999)
- [44] A. Boyd, M. Akay, B.J. Meenan, Surf. Interface Anal. 35, 188 (2003)
- [45] T.F. Stoica, C. Morosanu, A. Slav, T. Stoica,
 P. Osiceanu, C. Anastasescu, M. Gartner,
 M. Zaharescu, Thin Solid Films 516, 8112 (2008)
- [46] C. Battistoni, M.P Casaletto, G.M. Ingo, S. Kaciulis, G. Mattogno, L. Pandolfi, Surf. Interface Anal. 29(11), 773 (2000)
- [47] A.J. Nathanael, D. Mangalaraj, S.I. Hong, Y. Masuda, Mater. Charact. 62, 1109 (2011)
- [48] K.S.W. Sing, D.H. Everett, R.A.W. Haul, L. Moscou, R.A. Pierotti, J. Rouquerol, T. Siemieniewska, Pure Appl. Chem. 57, 603 (1985)
- [49] C. Zhang, C. Li, S. Huang, Z. Hou, Z. Cheng, P. Yang, Biomaterials 31, 3374 (2010)
- [50] S.J. Gregg, K.S.W. Sing, Adsorption, Surface Area and Porosity, 2nd edition (Academic Press, London, 1982)
- [51] Y. Liu, C.Y. Liu, J.H. Wei, R. Xiong, C.X. Pan, J. Shi, Appl. Surf. Sci. 256, 6390 (2010)
- [52] J. Leiser, B.A. Molitoris, Biochim. Biophys. Acta 1225, 1 (1993)
- [53] D.A. Parsell, S. Lindquist, Annu. Rev. Genet. 27,

- 437 (1993)
- [54] T.J. Webster, E.A. Massa-Schlueter, J.L. Smith, E.B. Slamovich, Biomaterials 25, 2111 (2004)
- [55] M. Kheradmandfard, M.H. Fathi, J. Alloys. Compd. 504, 141 (2010)
- [56] A. Bianco, I. Cacciotti, M. Lombardi, L. Montanaro, E. Bemporad, M. Sebastiani, Ceram. Int. 36, 313 (2010)
- [57] R.Z. Le Geros, G. Quirolgico, J.P. Le Geros, J. Dent. Res. 60B, 452 (1981)
- [58] J. Christoffersen, M.R. Christoffersen, N. Kolthoff, O. Barenholdt, Bone 20, 47 (1997)
- [59] C. Ergun, T.J. Webster, R. Bizios, R.H. Doremus, J. Biomed. Mater. Res. 59, 305 (2002)
- [60] G. Bonel, G. Montel, Compt. Rend. 258, 923 (1964)
- [61] R.Z. Le Geros, O.R. Trautz, J.P. Le Geros, E. Klein, Extrait du bulletin de la Societe' Chimique de France 1712 (1968) (in French)
- [62] C. Yang, P.P. Yang, W.X. Wang, J. Wang, M.L. Zhang, J. Lin, J. Colloid Interf. Sci. 328, 203 (2008)
- [63] Z.Y. Hou, P.P. Yang, H.Z. Lian, L.L. Wang, C.M. Zhang, C.X. Li, R.T. Chai, Z.Y. Cheng, J. Lin, Chem. Eur. J. 15, 6973 (2009)
- [64] I.R. Gibson, S.M. Best, W. Bonfield, J. Biomed. Mater. Res. 44, 422 (1999)
- [65] H. Owada, K. Yamashita, T. Umegaki, T. Kanazawa, M. Nagai, Solid State Ionics 35(3-4), 401(1989)
- [66] P. Dancker, I. Low, W. Hasselbach, T. Wieland, Biochim. Biophys. Acta. 400, 407 (1975)
- [67] Z. Spoerl, M. Stumpf, A.A. Noegel, A. Hasse, Oligomerization, J. Biol. Chem. 277(50), 48858 (2002)
- [68] K.J. Kelly, Contrib. Nephrol. 148, 86 (2005)
- [69] S.D. Westerheide, R.I. Morimoto, J. Biol. Chem. 280(39,) 33097 (2005)
- [70] F. Amorim, P.L. Moesley, In: A.A.A. Asea, B.K. Pedersen (Eds.), Heat Shock Proteins and Whole Body Physiology (Springer Science Business Media B.V., Dordrecht, Heidelberg, London, New York, 2010)
- [71] S.C. Gupta, A. Sharma, M. Mishra, R.K. Mishra, D.K. Chowdhuri Life Sci. 86, 377 (2010)
- [72] B.M. Sanders, L.S. Martin, Sci. Total Environ. 139-140, 459 (1993)
- [73] S.W.Y. Wong, P.T.Y. Leung, A.B. Djurišić,
 K.M.Y. Leung, Anal. Bioanal. Chem. 396, 609 (2010)
 M. Ahamed, R. Posqai, T.J. Gorey, M. Nielsen,
- [74] S.M. Hussain, J.J. Rowe, Toxicol. Appl. Pharmacol. 242(3), 263 (2010)
- [75] W.J. Chirico, M.G. Waters, G. Blobel, Nature 332, 805 (1988)

- [76] S.M. Van der Vies, A.A. Gatenby, P.V. Viitanen, G.H. Lorimer, In: J.L. Cleland (Ed.), Molecular chaperones and their role in protein assenbly. Protein folding in vivo and in vitro (American Chemical Society, Washington DC, 1993) pp. 72-83
- [77] K. Jimbow, Y. Tamura, A. Yoneta, T. Kamiya, I. Ono, T. Yamashita, A. Ito, H. Honda, K. Wakamatsu, S. Ito, S. Nohara, E. Nakayama, T. Kobayashi, J. Biomat. Nanobiotechnol. 3, 140 (2012)
- [78] J. Xu, P. Xu, Z. Li, J. Huang, Z.Yang, J. Biomed. Mater. Res. A 100(3), 738 (2012)
- [79] Z. Xu, C. Liu, J. Wei, J. Sun, J. Appl. Toxicol. 32(6), 429 (2012)